Artifact reduction in breast tomosynthesis by including prior knowledge of the compressed breast shape

Koen Michielsen*, Alejandro Rodriguez-Ruiz*, Greeshma Agasthya†, and Ioannis Sechopoulos*‡
* Dept. of Radiology and Nuclear Medicine, Radboud University Medical Center, Nijmegen, The Netherlands
† Dept. of Radiology and Imaging Sciences, Emory University, Atlanta, GA, USA
‡ Dutch Reference Centre for Screening (LRCB), Nijmegen, The Netherlands

***Abstract*—Due to the limited angle acquisition in breast tomosynthesis, it is susceptible to artifacts. One of these artifacts is caused by incomplete knowledge of the exact compressed breast shape and results in underestimation of attenuation values near the skin. To avoid this artifact, compressed breast shapes were measured using structured light scanning and this information was included in the reconstruction algorithm. Care was taken to accurately position the measured shape in the reconstruction geometry in order to avoid introducing different artifacts.**

Evaluation in phantom and patient reconstructions found that adding the exact breast shape greatly reduced the underestimation of attenuation values near the skin.

I. Introduction

Digital breast tomosynthesis (DBT) is a pseudo 3D imaging technique which acquires data over a limited angular range and reconstructs thick slices parallel to the detector. It improves visualization of soft tissue lesions by reducing the effect of overlapping anatomical structures, and has equal or better diagnostic performance than digital mammography [1], [2].

The incomplete knowledge due to the limited angular range can result in reconstruction artifacts [3]. In this work, we consider the specific artifact caused by the overestimation of the x-ray attenuation path length at the breast edge. This effectively spreads out the attenuation, resulting in an overestimation outside the breast, and an underestimation inside the breast, as can be seen in the uncorrected reconstructions in figures 3 and 4. Zhang et al. [4] propose a solution where the 3D breast shape is estimated by backprojecting the segmented 2D breast shape in each projection and this 3D shape is used to limit the overestimation of the x-ray path length. In this work, we demonstrate the use of the actual measured 3D breast shape [5] to reduce the reconstruction artifact.

II. Materials & Methods

A. Breast Shape Measurement

All participants provided informed consent, and the study was IRB approved and HIPAA compliant. Compressed breast shapes were measured for 50 women undergoing breast cancer screening or diagnostic work-up. The measurement was performed simultaneous to the acquisition of a cranio-caudal (CC) view on a Selenia Dimensions breast tomosynthesis system (Hologic Inc, Bedford, MA, USA).

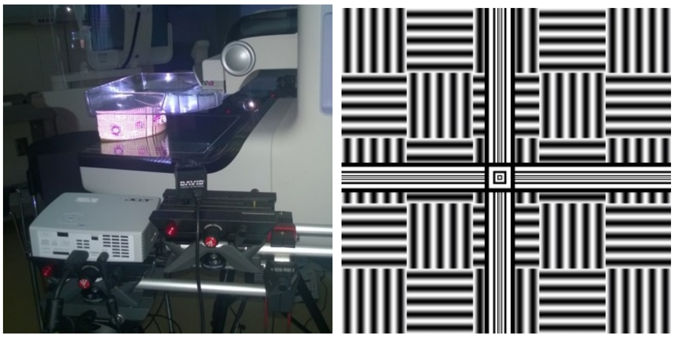

(a) Experimental setup. (b) Light pattern.

Figure 1: Photograph of the structured light scanning setup and an example of a structured light pattern.

Images of the compressed breast surface were acquired using two structured light scanning systems (figure 1a). Each system combines a digital projector (K132, Acer Inc, Xizhi, New Taipei, Taiwan) that projects 24 different patterns similar to the one shown in figure 1b onto the object of interest, with a digital camera (USB CMOS Monochrome Camera 3.1-M, David Visions Systems, Palo Alto, CA, USA) that captures the reflection of these patterns. Acquisition of the entire series of patterns takes approximately 7 seconds. The structured light scanning systems were placed to the left and right of the tomosynthesis unit in order to cover the entire breast without needing to reposition the cameras. After acquisition, each set of images is processed (DAVID-3 software, David Visions Systems, Palo Alto, CA, USA) to create a 3D representation of the surface of the scanned object. Since this technology uses a low intensity light source rather than laser light to project the patterns, no eye protection is needed. The compression paddle was covered with a thin opaque tape layer to avoid possible reflections.

The measured raw data from both cameras, as shown in figure 2a, were imported in the DAVID-3 software, and surfaces unrelated to the actual breast shape, such as the compression paddle or breast support plate, were removed manually (figure 2b). In the final step, data from both camera views were aligned and merged using global fine registration, with the result shown in figure 2c. A more detailed description

DOI: 10.12059/Fully3D.2017-11-3202037

of these measurements and an analysis of their accuracy has been submitted for publication [6].

B. Reconstruction with prior shape knowledge

The breast tomosynthesis projection data are reconstructed using the Maximum Likelihood for Transmission tomography (MLTR) algorithm [7]. As the name implies, the goal of the reconstruction is to find the most likely attenuation distribution $\vec{\mu}$, with μ_j the attenuation in voxel j, that explains measured data $\vec{y}$, with y_i the measured pixel value for projection line i, or in short, find $\arg\max_{\vec{\mu}} P\left(\vec{\mu}|\vec{y}\right)$. This maximum is found by performing the following update on the reconstruction volume:

$$\mu_j^{(n+1)} = \mu_j^{(n)} + \frac{\sum_i l_{ij}\left(\hat{y}_i^{(n)} - y_i\right)}{\sum_i l_{ij}\hat{y}_i^{(n)}\sum_k l_{ik}}, \tag{1}$$

with $\hat{y}_i^{(n)}$ the expected measurement in pixel i after n iterations, which is determined by applying the forward model to the current estimate of the attenuation distribution $\vec{\mu}^{(n)}$. All reconstructions in this work were initialized with $\mu_j^{(0)} = 0$. In the case of the MLTR algorithm, the forward model $\hat{y}_i$ is a basic mono-energetic transmission acquisition without scattered radiation:

$$\hat{y}_i\left(\vec{\mu}\right) = b_i e^{-\sum_j l_{ij}\mu_j}, \tag{2}$$

with l_{ij} the intersection length between projection line i and voxel j, and b_i the unattenuated value for projection line i.

This reconstruction can be easily modified to include the measured breast shape from section II-A by restricting the reconstruction volume to said shape. However, since performing calculations in a non-rectangular volume is not very practical, a weighting factor α, set to 1 inside the breast shape and 0 outside, is introduced in the update step:

$$\mu_j^{(n+1)} = \mu_j^{(n)} + \frac{\alpha_j\sum_i l_{ij}\left(\hat{y}_i^{(n)} - y_i\right)}{\sum_i l_{ij}\hat{y}_i^{n}\sum_k \alpha_k l_{ik}}, \tag{3}$$

so that updates outside the sub-volume determined by the measured breast shape are set to zero in each iteration. The practical implementation can be optimized by only calculating the updates within the selected sub-volume.

C. Evaluation

We examine the usefulness and feasibility of our method in two experiments, the first using a simulated phantom, and the second using patient data.

In order to verify the effect of our method in ideal circumstances, we simulated acquisitions of a homogeneous phantom with a shape based on the measured breast contours [6], [8] and attenuation set to 0.5 cm^{-1} inside the contour and 0.0 cm^{-1} outside. The projection data were generated for wide (50°) and narrow (15°) angle projection geometries, similar to the Siemens Mammomat Inspiration and Hologic Selenia Dimensions geometries respectively [9].

To show the influence of the specific artifact we try to address, an ideal simulation is performed according to the forward model in equation (2), excluding other causes of artifacts such as scatter and beam hardening. The phantom and reconstruction volumes contained 2560×1280×50 voxels of 0.1×0.1×1.0 mm^3. The other projection parameters are listed in table I.

Table I: Simulation Parameters

	Wide Angle (50°)	Narrow Angle (15°)
Number of projections	25	15
Detector size	3584×2816	2048×1664†
Detector pixel size	85×85 μm^2	140×140 μm^{2†}
Source-detector distance	655.5 mm	700 mm

† After 2×2 binning.

The projection data are reconstructed using 10 MLTR iterations with and without including the exact contour, i.e. following equations (3) and (1), respectively. Both reconstructions are then evaluated by inspecting the difference images of the reconstruction and the original phantom.

We demonstrate the practical feasibility of our method by applying it to one of the patient cases from section II-A. The selected scan was acquired with a total tube current-exposure time product of 77 mAs for 15 projections and a 36 kVp spectrum produced by a Tungsten target and filtered by 0.7 mm of Aluminum, and was reconstructed in a volume of 2048×1664×79 voxels of 0.14×0.14×1.0 mm^3, using the geometric parameters found in the DICOM header of the projection data.

The main difficulty was positioning the measured breast shape at the correct location in the reconstruction geometry. This alignment was done in two steps: first, the 3D shape was rotated and translated in 3D space so that it was located on the breast support plate, and then a further rotation and translation in 2D until the projection of the 3D shape was aligned with the 0° projection of the patient. Upon registration of the 3D shape and the 2D projection, the patient data was also reconstructed using 10 MLTR iterations with and without the measured breast shape. Since in this case no ground truth is available, evaluation was performed by plotting attenuation profiles and visual comparison of the reconstructed planes.

III. Results

A. Phantom Reconstruction

The central axial, coronal, and sagittal slices of the difference images between each reconstruction and the original phantom are shown in figure 3 for the wide angle Siemens geometry and the narrow angle Hologic geometry. It should be noted that the color scale is 20 times wider for the reconstructions without knowledge of the breast shape than those including the *a priori* shape information. In these images it is clear that including the breast shape in the reconstruction improves the algorithm's ability to correctly reconstruct attenuation values near the breast edge. The artifacts that underestimate attenuation inside the breast by assigning part of that attenuation to voxels outside the breast contour have been greatly reduced.

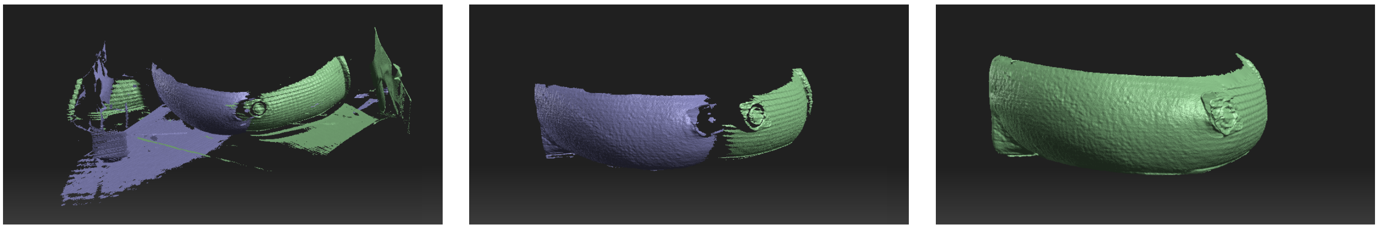

(a) Raw surface images acquired by the two scanning cameras.

(b) Cleaned images with signals that do not belong to the breast surface removed.

(c) Merged surfaces from both lateral cameras after fusion using global fine registration.

Figure 2: Post processing steps of the 3D external breast surface.

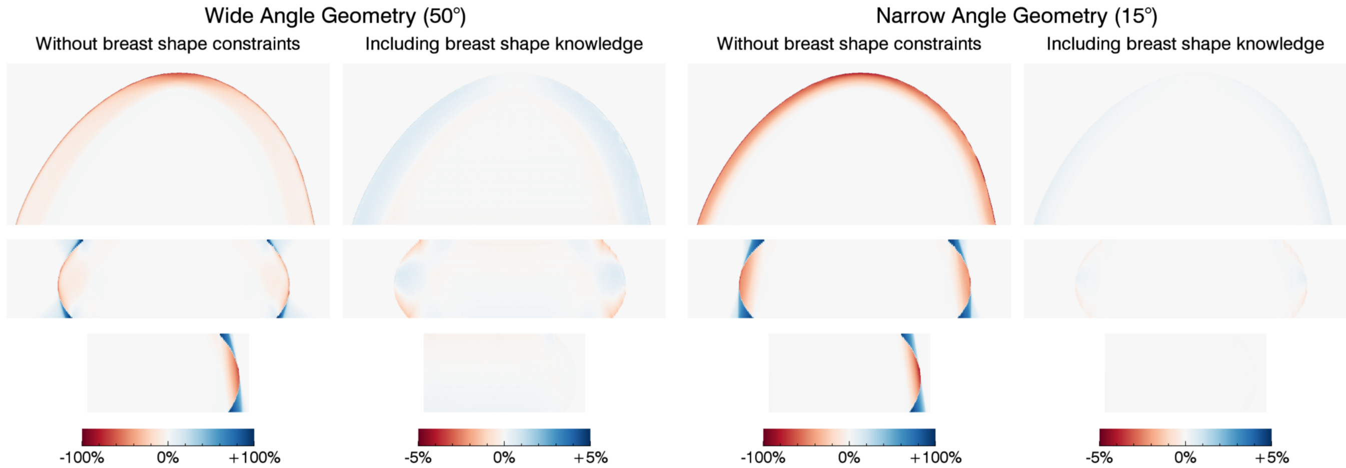

Figure 3: Central axial, coronal, and sagittal slices of the difference between the reconstructions with and without knowledge of the breast shape for wide angle and narrow angle geometries. Note the differences in the color scales.

When comparing the artifact appearance in wide and narrow angle geometries in figure 3, we find that for the wide angle geometry the area where attenuation is underestimated is larger while the error is smaller. In the narrow angle geometry, the area is smaller but the error is larger. After including the information on the exact breast shape, the artifact is greatly reduced in both cases, with the color scale in those images now covering an interval which is 20 times smaller. Here we can see that the artifact is almost completely gone in the narrow angle geometry, while it remains slightly visible in the wide angle geometry.

B. Patient Reconstruction

A reconstructed slice of a patient case is shown in figure 4, showing both reconstructions. It is clear that the underestimation of attenuation near the skin line is mostly resolved. This can be even better appreciated in the attenuation profile plotted in figure 5.

However, as can be seen in figure 6, a reconstructed slice close to the top of the breast, three distinct artifacts appeared after including breast shape information. The first is caused by the coarse 1 mm steps in the z-direction of the compressed breast shape that models the effect of the tilted compression paddle and can be seen as the lines going from top left to right bottom in this image. The compression paddle is usually assumed to be parallel to the detector cover in order to avoid this artifact. The second artifact can be seen as the overestimated attenuation of the skin line in the top left corner, and is probably caused by a slight misalignment of the measured breast shape in the reconstruction geometry. The third artifact, the dark area close to the nipple, is probably a part of the original artifact we tried to avoid, caused by overestimating the extent of the breast shape close to the compression paddle.

IV. Discussion

The results show that including the measured compressed breast shape helps in improved visualization of the subcutaneous breast tissue, specifically by allowing the viewer to choose a single window that shows the entire breast with optimal contrast. In reality our current setup is not a practical solution due to the need for additional hardware and lengthy post processing of the data. There is however no fundamental problem that would stop integration of a structured light scanning system in a tomosynthesis unit or full automation of the post processing.

Although the inclusion of the breast shape in the reconstruction process does not necessarily add further diagnostic information, it does improve the quantitative aspects of the reconstructed attenuation and will allow for better visualiza-

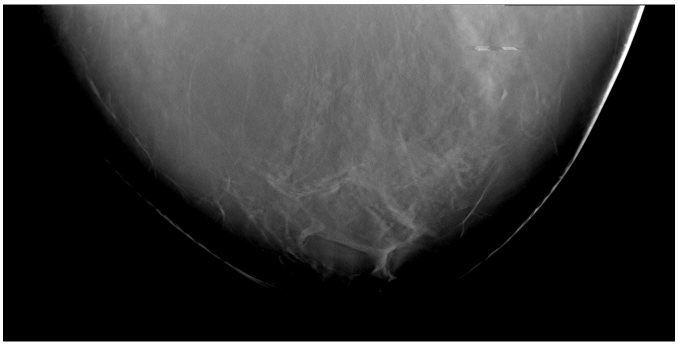

(a) Reconstruction without shape information.

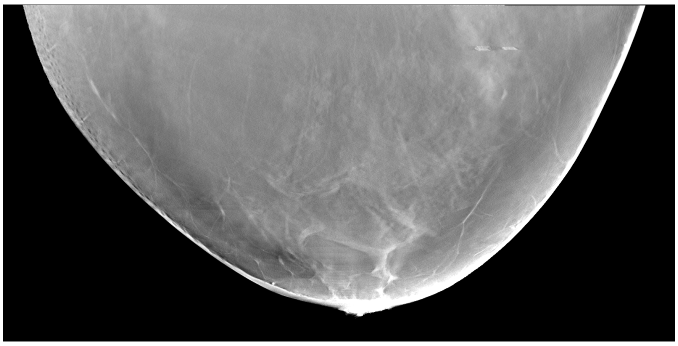

(b) Reconstruction with shape information.

Figure 4: Slice of the reconstructed patient. Window set to [0.2 cm^{-1} – 0.4 cm^{-1}] in both cases.

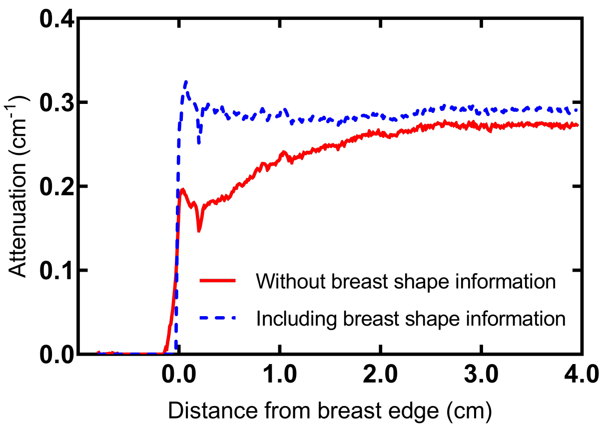

Figure 5: Attenuation profile near the skin line.

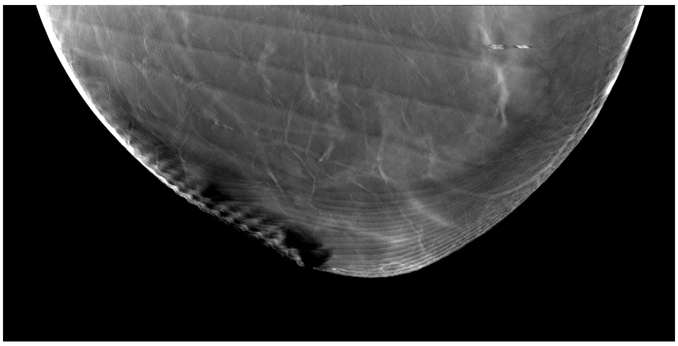

Figure 6: Artifacts in a reconstruction with shape information. Window set to [0.25 cm^{-1} – 0.35 cm^{-1}].

tion of the reconstructed information. Even though we only demonstrate its usefulness for the MLTR method, the shape information may be used with any iterative reconstruction, and could potentially be useful for FBP methods that do not completely filter the zero frequency.

The artifacts in figure 6 suggest the main improvements needed in our method. In first instance, the positioning of the measured breast shape in the reconstruction geometry needs to be as precise as possible. In the future, measurements could be performed by an integrated system, where known positions for each component make registration straightforward. For now, inclusion of a third camera would add robustness to the registration of the raw surfaces and markers could be added to the compression paddle and detector cover to make it easier to correctly place the measured shape in the reconstruction volume. The sawtooth artifact should be reduced by creating smoother changes in thickness of the measured shape, e.g. by allowing the voxel height in the top layer to vary through the plane.

The initial phantom experiment shows an interesting difference between wide and narrow angle acquisitions. Before correction, the narrow angle system shows a more severe underestimation of the attenuation concentrated close to the skin edge, while the wide angle system shows less underestimation, but over a larger area. In both instances the artifact was reduced after including shape information, but less so for the wide angle acquisition than the narrow angle acquisition. It seems unlikely that this aspect was considered during system design since it does not appear in FBP reconstructions where the zero-frequency is filtered out completely.

To conclude, we show that we can add information from the measured compressed breast shape information to the breast tomosynthesis reconstruction to produce more accurate attenuation values near the breast edge.

Acknowledgments

Supported in part by Grants No. R01CA163746 and R01CA181171 from the National Cancer Institute, National Institutes of Health and Grant No. IIR13262248 from the Susan G. Komen Foundation for the Cure. The content is solely the responsibility of the authors and does not necessarily represent the official views of the National Cancer Institute, the National Institutes of Health of the Komen Foundation. The authors would like to acknowledge Ellen D'Orsi for the patient recruitment and imaging.

REFERENCES

[1] N. Houssami and P. Skaane, "Overview of the evidence on digital breast tomosynthesis in breast cancer detection," *Breast*, vol. 22, no. 2, pp. 101–108, Feb. 2013.

[2] J. Lei, P. Yang, L. Zhang, Y. Wang, and K. Yang, "Diagnostic accuracy of digital breast tomosynthesis versus digital mammography for benign and malignant lesions in breasts: a meta-analysis," *Eur. Radiol.*, vol. 24, no. 3, pp. 595–602, Mar. 2014.

[3] I. Sechopoulos, "A review of breast tomosynthesis. part II. Image reconstruction, processing and analysis, and advanced applications," *Med. Phys.*, vol. 40, no. 1, p. 014302, Jan. 2013.

[4] Y. Zhang, H.-P. Chan, B. Sahiner, Y.-T. Wu, C. Zhou, J. Ge, J. Wei, and L. M. Hadjiiski, "Application of boundary detection information in breast tomosynthesis reconstruction," *Med. Phys.*, vol. 34, no. 9, pp. 3603–3613, Sep. 2007.

[5] G. Agasthya and I. Sechopoulos, "TU-CD-207-09: Analysis of the 3-D Shape of Patients' Breast for Breast Imaging and Surgery Planning," *Med. Phys.*, vol. 42, no. 6, pp. 3612, Jun. 2015.

[6] A. Rodriguez-Ruiz, G.A. Agasthya, and I. Sechopoulos, "The compressed breast during mammography and breast tomosynthesis: in vivo shape characterization and modeling," *Phys. Med. Biol.*, under review.

[7] J. Nuyts, B. De Man, P. Dupont, M. Defrise, P. Suetens, and L. Mortelmans, "Iterative reconstruction for helical CT: a simulation study," *Phys. Med. Biol.*, vol. 43, no. 4, pp. 729–737, Apr. 1998.

[8] A. Rodríguez-Ruiz, S.S.J. Feng, J. van Zelst, S. Vreemann, J. Rice Mann, C.J. D'Orsi, and I. Sechopoulos, "Improvements of an objective model of compressed breasts undergoing mammography: Generation and characterization of breast shapes," *Med. Phys.*, (online preprint) Feb. 2017.

[9] I. Sechopoulos, "A review of breast tomosynthesis. part I. The image acquisition process," *Med. Phys.*, vol. 40, no. 1, p. 014301, Jan. 2013.